Modeling and Optimized Gait Planning of Biped Robots with Different Leg Mechanisms

Behnam Dadashzadeh[1*], Akbar Allahverdizadeh[1], Mehdi Azhdarzadeh[2]

1- Department of Mechatronics Engineering, University of Tabriz, Tabriz, Iran
* 29 Bahman Blvd., ZIP Code: 5166616471 Tabriz, Iran, b.dadashzadeh@tabrizu.ac.ir
2- University of Alberta, Edmonton, Canada

Abstract

This research focuses on modeling and gait generation optimization of four different real biped models that include practical extended models of the theoretical SLIP and compass gait as a novelty of the work. The first model is kneed Biped model without spring that is a 5-rigid-link robot with four actuators in its hip and knees. The second model, kneed biped model with springs in shins is very similar to the first model, but its shins have linear springs. The 3rd model is a semi-telescopic springy biped model and the 4th model is a semi-compass gait with kneed swing leg. Optimization parameters of their walking gait, objective functions and constraints are presented and successive stages of optimization are completed to find the optimal gaits. The efficiency of the gaits and required motor torques for the optimal gait of each model are illustrated.

Keywords: Biped Robot, Walking, Dynamic Modeling, Gait Planning, Optimization, Leg Mechanism, Kneed, semi-Telescopic, Semi-Compass.

1. Introduction

A wide range of applications has been predicted for biped robots. These robots have lots of advantages such as adaptability with surroundings, high maneuverability, and demonstrating a better energy performance in dynamic walking gait (specifically biped robots with point feet). Biped robots are categorized into two groups of active and passive. Passive robots have advantages such as their minimum energy use, hence being economical energy-wise, lack of complexity in design and build, and giving an idea for the design of active robots. They also have some disadvantages such as limitation in motion, instability to external perturbations, and special environment requirement. Developing humanoid and animal-like robots that mimic the real case in kinematics, kinetics, and physiologic structure is very challenging. For example, humans are capable of doing a wide range of dynamic maneuvers with lots of complexities in different environments and at the same time handling external perturbations.

To build a robot comparable to humans from efficiency, stability and strength point of view, it is required to have a better understanding of human walking. Therefore, a variety of models for human walking have been proposed and it is demonstrated that the simple passive SLIP (Spring Loaded Inverted Pendulum) model can mimic human motion on a flat surface more closely (Geyer et al., 2006). Energy consumption is another important factor in robot design. The problem of optimum gait for a robot, considering energy expenditure is usually formulated as a standard energy optimization problem. There are a couple of popular methods such as the shooting method (Rostami & Bessonnet, 2001) and parameter optimization method (Saidouni & Bessonnet, 2003).

(Rummel et al., 2010) used a bipedal spring-mass model as the base of their model. This model predicts hip movement, single and double support phase and reaction force of the ground accurately. They investigated the effect of attack angle for the leg and its stiffness and showed that symmetrical gait with a smaller angle of attack will result in a better compromise between gait robustness and energy efficiency. They also demonstrated that there is a direct relationship between higher stiffness and robustness of walking gaits. (L. C. Visser et al., 2013) proposed a hybrid model for a biped walker with variable leg stiffness and a control strategy for a stable gait. They also showed that this control strategy is energy efficient.

(Hao et al., 2020) applied generating functions approach to an unconstrained biped robot to get optimum gaits. He also developed a PD controller to reduce the modeling error. (Bauer et al., 2016) optimized the walking energy efficiency of biped using elastic couplings at 0.3 to 2.3 m/s speed ranges. (Kai & Shibata, 2015) developed a unique method based on the nonlinear optimization technic and discrete mechanics for compass-type biped on irregular grounds. They formulated a discrete gait generation method on the irregular ground and optimized it using the nonlinear control strategy with finite dimensions. Then, they proved their method for generating a stable gait for the CCBR (Continuous-time Compass-type Biped Robot) on irregular grounds. (Liu et al., 2019) developed a novel chattering-free pi sliding mode control for compass gait biped model that is a nonlinear underactuated system.

(Srinivasan & Ruina, 2006) used a model to describe walking and running with an infinite variety of gaits. Simple optimization methods showed that biped motion can be controlled extensively via control of work performed of the legs. (Rokbani & Alimi, 2012) introduced an approach that can generate a gait for biped robots. Their method is combing a classic dynamic model with an inverse kinematic solver based on Particle Swarm Optimization (PSO). (Adolfsson et al., 2001) studied a passive three-dimensional model with ten degrees of freedom using simple models (McGeer & Alexander, 1990). Their model includes force discontinuities and instantaneous changes like impact in state variables. (Millard et al., 2011) focused on examining a control system that allows the robot to move at constant speeds like a human. Although the kinematics of the final model was very similar to the kinematic of human joints, the reaction force profile of the ground was different. (S. Shimmyo et al., 2010) used preview control with the virtual plane method to generate a pattern of walking. Using preview control, errors related to simple models can be reduced. With their developed pattern, model errors can be reduced directly and without using the preview control method. (Martin & Schmiedeler, 2014) studied four and six-link planar models with knee and rigid circular feet. The difference between the four and six-link models was the addition of ankle to the six-link model. They generated stable walking gaits for both models using the hybrid zero dynamics-based method. Compared to human walking, the six-link model could match closely, but the four-link model could not, which highlights the importance of the ankle in human walking. (Gamus & Or, 2015) investigated the hybrid dynamics of biped robots under slip-stick transitions of foot. They worked on two simple planer models with point feet including a rimless wheel and a compass biped. (Mandava et al., 2019) generated balanced gaits of a biped robot on stairs and sloping surfaces using an analytical approach.

This research focuses on modeling, optimization, and gait generation of four different biped models. The models are the kneed biped model without spring, kneed biped model with spring in shins, semi-telescopic springy biped model, and semi-compass gait biped with kneed swing leg. These models are based on the TARMER (Tabriz Running Mechatronical Robot) that has been fabricated by our team with the capability of executing these gaits. This robot is shown in Fig. 1. Optimization is done based on the COT (Cost Of Transport) and periodic gait error improvement. The main contribution of this paper is developing novel practical extended models of the theoretical SLIP and compass gait models and comparing their efficiencies to the standard kneed model. These extended models have not been investigated in the previous works. Resulted different gaits for these biped models are compared and discussed based on the COT and required motor torques.

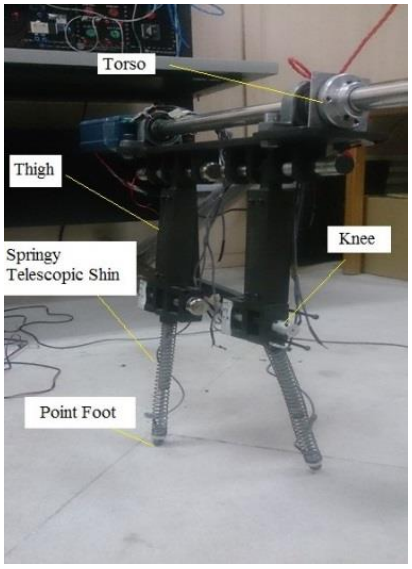

Fig. 1. The TARMER robot with lockable springy legs

2. Robot Models

2.1 Kneed robot model without spring

The first model is a robot with kneed leg and without spring. Each link for thigh and shin consists of a bar with a known mass, center of mass, and moment of inertia. Mass of the torso is assumed to be concentrated in the hip joint. Walking gait is composed of the single support phase, touch-down event, double support phase, and take-off event.

2.1.1 Single support phase

As shown in Fig. 2, in the single support mode, point A is a pivoted connection and robot has four degrees of freedom, assuming a locked torso angle. Components of the generalized coordinates for this phase, angles of the links, are $[\boldsymbol{q}_{ss}]_{4\times1}$. Locations of the COM (Center of Mass) of the links and torso are described in terms of the generalized coordinates. Linear and angular velocities of the COM of the links are written as a function of the time derivative of the generalized coordinates. It is assumed that the robot's body is constrained for rotation by a boom, so its angular velocity is zero. To use the Lagrangian equation to derive the equations of motion, kinetic and potential energies are calculated

$$T = \frac{1}{2}\sum_i (m_i {v_i}^2 + I_i {\omega_i}^2) \quad (1)$$

$$V = \sum_i m_i g h_i \quad (2)$$

where v is the velocity of the COM in m/s, ω is the angular velocity in rad/s, m is the mass in kg, I is the moment of inertia in $kg.m^2$ and h is the height of the COM in m.

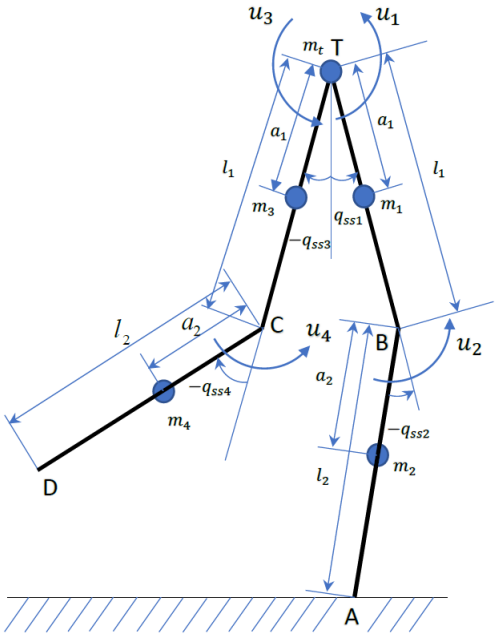

Fig. 2. Kneed biped without spring in single support configuration.

Using the Lagrangian function as $L = T - V$, Lagrange equation is

$$\frac{d}{dt}\left(\frac{\partial L}{\partial \dot{q}_i}\right) - \frac{\partial L}{\partial q_i} = Q_i, i = 1,2,3,4 \qquad (3)$$

where q_i is the ith component of the generalized coordinates. Neglecting friction in the joints and applying the virtual work method, the generalized forces, Q_i, will be

$$Q_1 = u_1, Q_2 = u_2, Q_3 = u_3, Q_4 = u_4 \qquad (4)$$

After intruding Eq. 4 into Eq. 3, the general dynamic model of the stance phase will be

$$[D_{ss}(q_{ss})]_{n\times n}[\ddot{q}_{ss}]_{n\times 1} + [C_{ss}(q_{ss}, \dot{q}_{ss})]_{n\times 1} = [B_{ss}]_{n\times m}[u_{ss}]_{m\times 1} \qquad (5)$$

In the equation above $D_{ss}(q_{ss})$ is the matrix of inertia and $C_{ss}(q_{ss}, \dot{q_{ss}})$ encompass Coriolis, gravity, and elastic effects. The degree of freedom is $n = 4$, the number of control inputs is $n = 4$ and u_{ss} is the input vector composed of torque of the motors. B_s matrix results from Eq. 4 as follows

$$B_s = \begin{bmatrix} 1 & 0 & 0 & 0 \\ 0 & 1 & 0 & 0 \\ 0 & 0 & 1 & 0 \\ 0 & 0 & 0 & 1 \end{bmatrix} \qquad (6)$$

The state vector is defined as $x_{ss} = [q_{ss};\ \dot{q}_{ss}]$ and four second-order differential equations resulted from Eq. 5 are rewritten as eight first-order differential equations that will be the state equations as follows.

$$\dot{x}_{ss} = f_{ss}(x_{ss}) + g_{ss}(x_{ss}).u_{ss} \qquad (7)$$

where

$$f_{ss}(x_{ss}) = \begin{bmatrix} \dot{q}_{ss}(x_{ss}) \\ -{D_{ss}}^{-1}(x_{ss}).\, C_{ss}(x_{ss}) \end{bmatrix} \quad (8)$$

$$g_{ss}(x_{ss}) = \begin{bmatrix} 0_{n\times m} \\ {D_{ss}}^{-1}(x_{ss}).\, B_{ss} \end{bmatrix} \quad (9)$$

These equations are solved numerically by MATLAB.

2.1.2 Double support phase

The double support phase for this model is a two degree of freedom model. In this configuration, the motion of the front leg is fully dependent on the rear leg which is the reference leg. This method is an alternative to the method of using equations with four degrees of freedom and two constraint equations on the single support phase equations. The generalized coordinates and angles for the front leg are depicted in Fig. 3. Stride length, a, is the distance of legs' toes on the ground in the double support phase. This distance is known from the final condition of the single support phase.

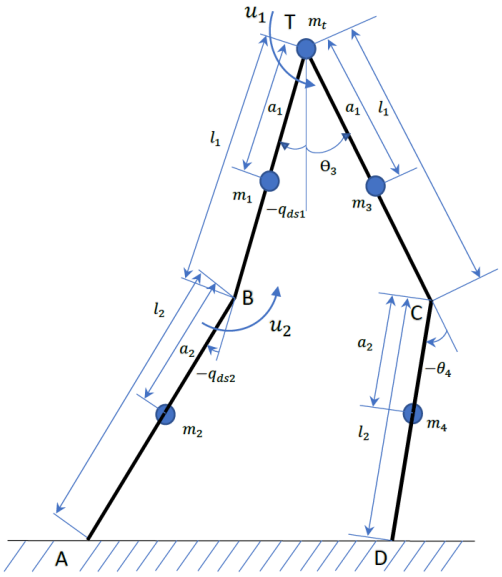

Fig. 3. Double support phase for kneed biped without spring.

Using Fig. 3, x_T and y_T are written in terms of the generalized coordinates by assuming the origin of the coordinates in point A. Then, to get θ_3 and θ_4 for the front leg in terms of the generalized coordinates (q_{ds1}, q_{ds2}), geometric relations from the triangle made by the front leg and ground is used. The dynamic equation of this 2 DOF system is written as follows, in which $n = 2$ and $m = 2$.

$$[D_{ds}(q_{ds})]_{n\times n}[\ddot{q}_{ds}]_{n\times 1} + [C_{ds}(q_{ds}, \dot{q}_{ds})]_{n\times 1} = [B_{ds}]_{n\times m}[u_{ds}]_{m\times 1}. \quad (10)$$

2.1.3 Energy performance of the robot

Mechanical energy consumption of a mechanism with rotational actuators is written as, (Dadashzadeh et al., 2014)

$$W_{total} = \sum_{i=1}^{m} \int_0^{t_{step}} |\dot{\theta}_i . u_i| \, dt. \quad (11)$$

In this equation, u_i, $\dot{\theta}_i$ and t_{step} are the number of the motors, torque of the motors, angular velocity of the motors and the time needed for one step including both single and double support phases. The COT is defined as the energy used per unit of weight per distance traveled.

$$COT = \frac{W_{total}}{m_{total} . g . a} \quad (12)$$

where m_{total} is the sum of all parts used in the robot.

2.2 Kneed robot model with springy shin

This model is a kneed biped where shins are telescopic springy, and only the hip and knees joints are active. Each link has mass and moment of inertia. The only difference with the previous model is in the springy shin that adds one passive joint and one degree of underactuation to the system in the single support phase and two degrees in the double support phase. The method of deriving governing equations is similar to the previous model.

2.2.1 Single Support Phase

This robot model has 5 DOF in this phase and its schematic view is similar to Fig. 2 with a variable length of AB segment which is assumed as the third component of the generalized coordinates for this phase. q_{ss1} and q_{ss2} are angles of stance leg links and q_{ss4} and q_{ss5} are angles of swing leg links similar to the previous model. By calculating the linear and angular velocity of the links total kinetic energy of the robot is written using Eq. (1) and (2). The potential energy of the robot is calculated as

$$V = \sum_{i=1}^{5} m_i g h_i + \sum_{j=1}^{2} \frac{1}{2} k_j x_j^2 \quad (13)$$

where, h is the height of the COM for each component in m, k is the spring constant in N/m, and x is the change of the length of the spring in m.

Similar to the previous model, the dynamic equation of this model in the stance phase is written as Eq. (5), in which $n = 5$ and $m = 4$. B_{ss} matrix for this model is

$$B_{ss} = \begin{bmatrix} 1 & 0 & 0 & 0 \\ 0 & 1 & 0 & 0 \\ 0 & 0 & 0 & 0 \\ 0 & 0 & 1 & 0 \\ 0 & 0 & 0 & 1 \end{bmatrix}. \quad (14)$$

2.2.2 Double Support Phase

The kneed springy shin biped model in the double support phase is a four degree of freedom model whose generalized coordinates components are depicted in Fig. 4. q_{ds3} and q_{ds4} are the lengths of springy shins that vary due to their passive joints. Stride length, a, is a known parameter.

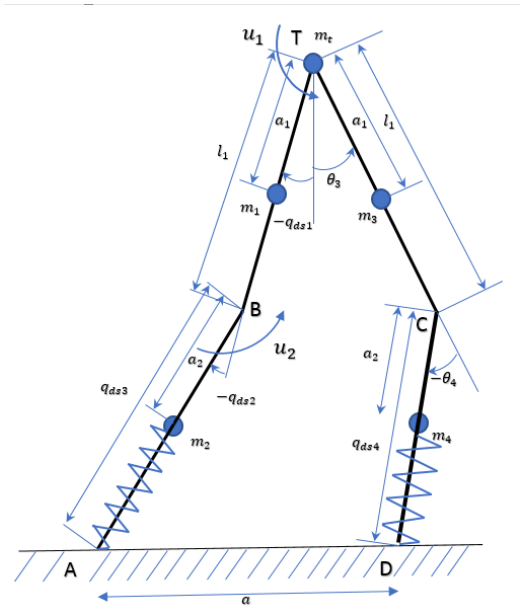

Fig. 4. Kneed springy shin biped in the double support phase.

The position of the torso is written as a function of the generalized coordinates. Then using triangle TCD and law of the cosines, the angles θ_3 and θ_4 of the second leg can be written as a function of q_1 , q_2, q_3 and q_4.

$$\theta_3 = tan^{-1}\left(\frac{a - q_3\, sin(-q_2 - q_1) - l_1\, sin(-q_1)}{Y_A + q_3\, cos(-q_2 - q_1) + l_1\, cos(-q_1)}\right) + cos^{-1}\left(\frac{{l_1}^2 - {q_4}^2 + \overline{TD}^2}{2l_1\overline{TD}}\right) \quad (15)$$

$$\theta_4 = \pi - cos^{-1}\left(\frac{{l_1}^2 + {q_4}^2 - \overline{TD}^2}{2l_1 q_4}\right) \quad (16)$$

Again, using the Lagrange equation, the dynamic model of this phase is derived as Eq. (10) in which $n = 4$ and $m = 2$.

Applied ground reaction forces to the toes are calculated by simultaneously solving Newton-Euler equations of all the links, having their velocities and accelerations known in each instance. These forces are used to detect a take-off event that ceases the double support phase.

2.2.3 Touch-down

When the stance leg of the robot in the single support phase swings forward and hits the ground, the single support state turns into a double support state. In this instance, ground impacts cause changes in the velocities of the links. Impact equation is written as

$$D_{ss}(q_{ss}).(\dot{q}_{ss}^{+} - \dot{q}_{ss}^{-}) = \hat{Q} \quad (17)$$

where D_{ss} is the inertia matrix of the single support phase. At touch-down instance, impact force $\hat{F}$ at point D is exerted perpendicular to the springy leg link (Hu et al., 2011) making angle $-\theta_4 - \theta_3$ with ground line according to Fig. 4. Virtual work resulted from this force can be written as

$$\sum_{i=1}^{5}\left(\hat{F}_x\frac{\partial x_D}{\partial q_i} + \hat{F}_y\frac{\partial y_D}{\partial q_i}\right)\delta q_i = \sum_{i=1}^{5}\hat{Q}_i\delta q_i \quad (18)$$

where q_i is the ith component of the variable $\boldsymbol{q}_{ss}$ and, x_D and y_D are functions of $\boldsymbol{q}_{ss}$. Although there is an impact force applied to the leg 1 at pivoted point A, its virtual work is zero because of the zero displacement of the pivoted joint. Eq. (18) along with constraint equations of switching the generalized coordinates between the single support and double support phase, constitute touch-down map. Solving them together results in the post-impact velocities that are used as the initial condition of the next phase.

2.3 Springy semi-telescopic leg robot model with kneed swing leg

In the current study, the theoretic telescopic leg biped model was extended to a semi-telescopic leg robot model with a kneed swing leg to ensure clearance of swing leg from the ground and make the model practical. In this robot model according to Fig. 5, during the single support phase, the stance leg has a straight telescopic springy joint. The swing leg at first has a knee to swing forward and clear the ground and later when the shin is aligned with the thigh, the angle for the swing leg is locked and remains straight until touch-down. Then the double support phase is started, and both of the legs are springy telescopic. The dynamic model of the stance phase is derived as Eq. (5) with $n = 4$ and $m = 3$ for the first sub-phase, and $n = 3$ and $m = 2$ for the second sub-phase. In the double support phase, it is derived as Eq. (10) with $n = 2$ and $m = 1$. For the details of deriving the equations for this type of robot, refer to (Dadashzadeh et al., 2019).

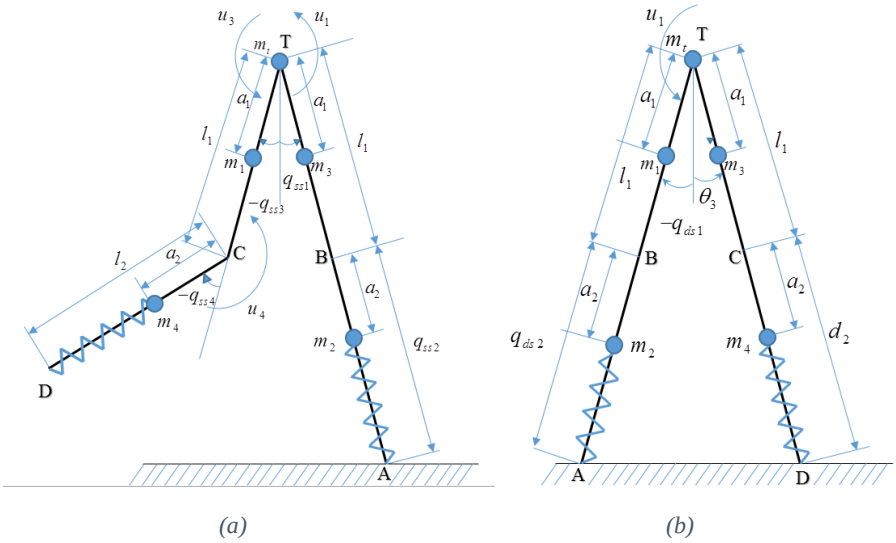

Fig. 5. Springy semi-telescopic leg robot model with kneed swing leg in (a) single support and (b) double support phase.

2.4 Semi-compass gait robot model with kneed swing leg

As shown in Fig. 6, this model is similar to the previous model, but it does not have any springs. Also, this model does not have a double support phase as the single support phase switches to the next single support phase by an instantaneous touch-down event. Details of deriving equations for this robot can be found in the research conducted by (Dadashzadeh et al., 2019).

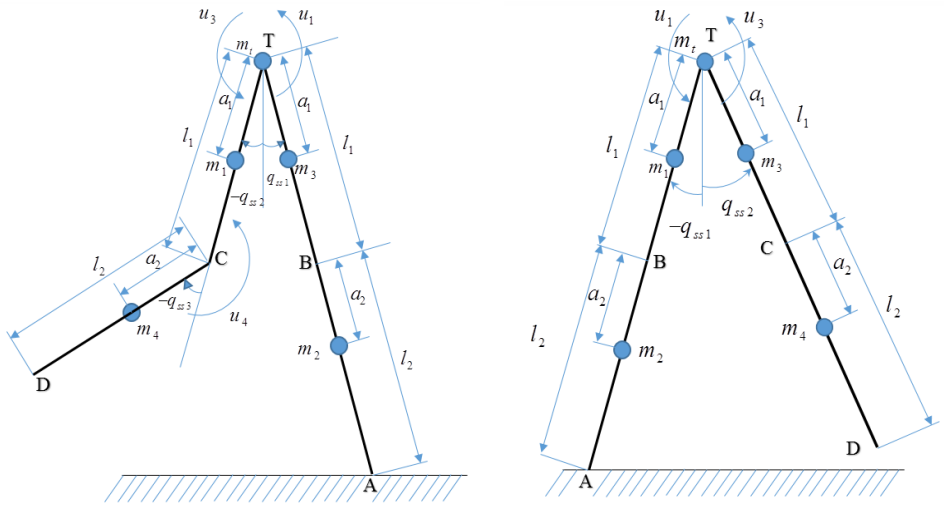

Fig. 6. Semi-compass gait robot model with kneed swing leg in the (a) first and (b) second sub-phase of single support phase.

3. Gait Generation by Optimization

To generate optimal gaits, two targets are considered for optimization. The first target is a periodic gait considering the error created between system states at the beginning of the gait and the end of the walking gait. The other target is optimizing the energy consumption of the robot's motors during the gait.

3.1 Kneed biped model without spring

The optimization approach for the kneed biped robot is described here and the same approach applies to the rest of the models. The motors' torque functions are discretized as a first-order hold function with 4 points, i.e. the discrete points are linearly interpolated to calculate torque value at any time. OP (Optimization Parameters) vector for one complete step of this robot model is considered as

$$\begin{aligned} OP = [&x_{ss_1}, x_{ss_2}, x_{ss_3}, x_{ss_4}, \dot{x}_{ss_1}, \dot{x}_{ss_2}, \dot{x}_{ss_3}, \dot{x}_{ss_4}, \\ &U_{ss_{11}}, U_{ss_{12}}, U_{ss_{13}}, U_{ss_{14}}, U_{ss_{21}}, U_{ss_{22}}, U_{ss_{23}}, U_{ss_{24}}, \\ &U_{ss_{31}}, U_{ss_{32}}, U_{ss_{33}}, U_{ss_{34}}, U_{ds_{11}}, U_{ds_{12}}, U_{ds_{13}}, U_{ds_{14}}, \\ &U_{ds_{21}}, U_{ds_{22}}, U_{ds_{23}}, U_{ds_{24}}] \end{aligned} \tag{19}$$

where, for example in motor torque $U_{SS_{13}}$, subscripts SS stands for the Single Support phase, number 1 is the motor number and number 3 means the third point from four points of the first-order hold torque function, and ds shows the double support phase.

The objective function considered for the optimization is the sum of the state error and energy expenditure function. Fig. 7 shows the optimization process for our first biped model and Fig. 8 shows optimized input torque for all motors during one complete step. Jumps of the torque values after 0.2 s is due to the phase change from single support to double support. The torque of motor 1, which is the motor actuating the hip of the stance leg, shows large values because it moves the robot forward. Also, motor 3 shows high values of positive and negative values as it accelerates and decelerates the thigh of the swing leg to move forward. Motors 3 and 4 are off in the double support phase.

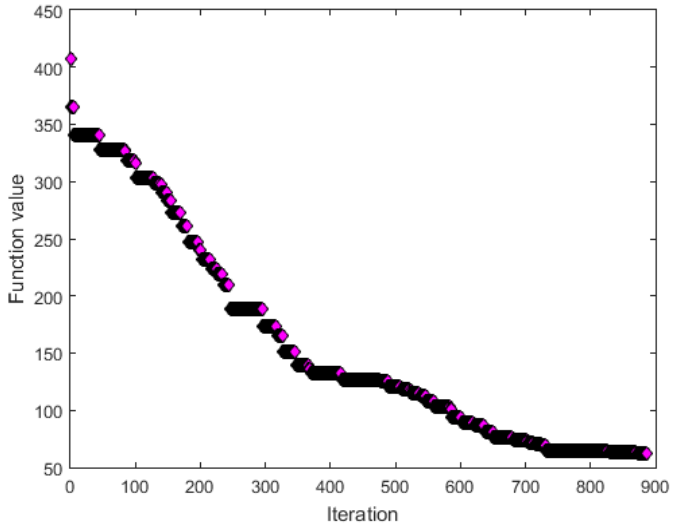

Fig. 7. Optimization process for the kneed biped robot.

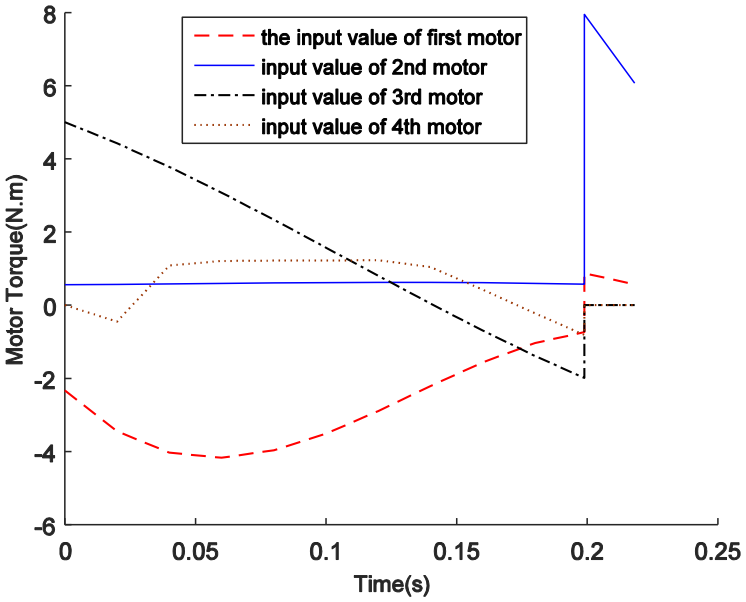

Fig. 8. Motors torque profiles for the kneed biped robot.

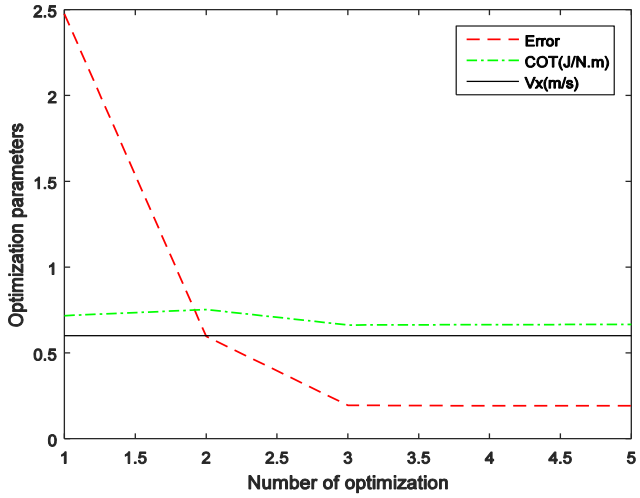

Fig. 9. Error variation, cost of transport and linear velocity of the kneed biped robot during the optimization process

Because the dynamic model is highly nonlinear with discontinuities, its optimization solution is likely trapped in local minimums. To resolve this problem, successive optimizations were used whose start points are the final points of the previous optimization. Fig. 9 shows the progression of the successive optimizations. The velocity in x direction remains constant, because of the penalty function. The red curve shows the change in the state error which is reduced substantially during 5 times optimization. COT function also shows a smooth drop. The Stick diagram of the robot for the resultant gait is shown in Fig. 10. The COM path in this gait is a curve with a very large radius of curvature that looks like a line in the figure. The phase diagram of the thigh is shown in Fig. 11 where it shows a periodic motion. This model generates an efficient gait with a COT of 0.66.

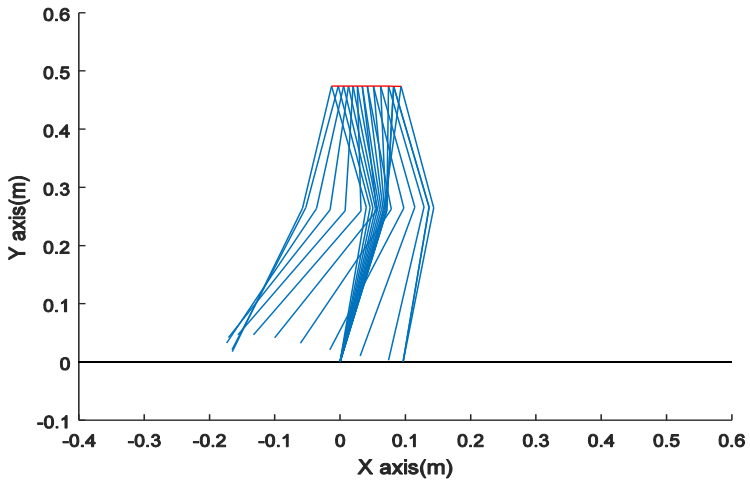

Fig. 10. Stick diagram of the resultant walking gait for the kneed biped robot.

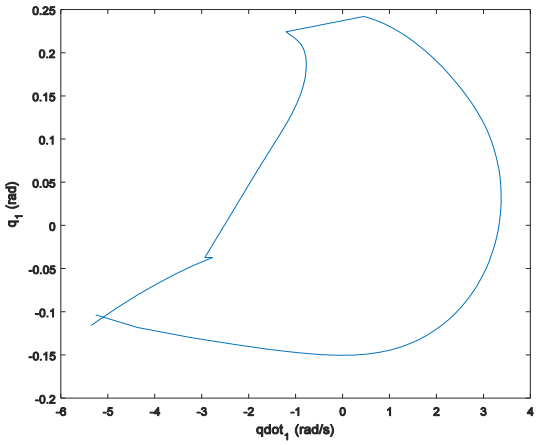

Fig. 11. Phase diagram for the thigh of the kneed biped robot

3.2 Kneed biped robot with Springy shins

Due to the high degrees of underactuation and passive motion of the springs in this robot model, gait optimization was very challenging. Therefore, the gait generated for this robot after several stages of optimization has a COT of 4.2, which is not very efficient. Fig. 12 shows the stick diagram of the resultant walking gait for this robot model.

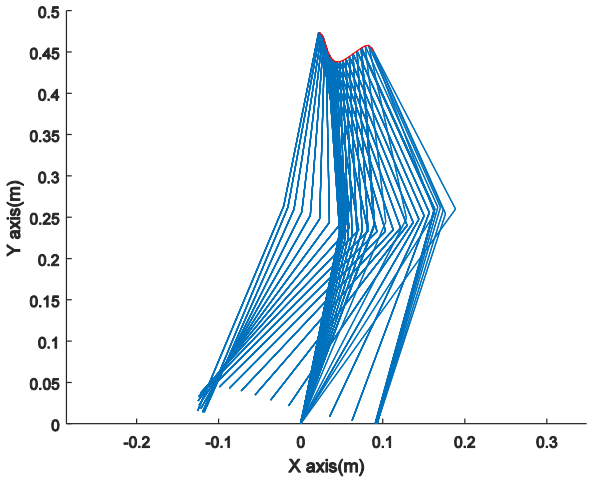

Fig. 12. Stick diagram for the kneed biped robot with spring legs

3.3 Springy semi-telescopic leg robot with kneed swing leg

Successive optimization processes are used to generate optimal gait for this robot model. The resultant motor torques after successive optimization stages are shown in Fig. 13. Two discontinuity points are noticed in the graph. The first one is due to the switching between the sub-phases of the single support phase, in which the swing leg is straightened and locked. The second one is at the touch-down event and switching to the double support phase. The torque of motor 1, which is controlling the thigh of the stance leg, shows a negative peak value at the beginning of the single support phase to accelerate the robot. The

torque of motor 2 is zero since the knee is locked. The torque of motor 4, which is controlling the motion of the shin of the swing leg, is constant in all cases because this joint has a fixed planar trajectory.

Fig. 14 shows the stick diagram of the walking gait of this robot. This gait generates a bigger stride length than the kneed models, but it has a larger COT equal to 1.09.

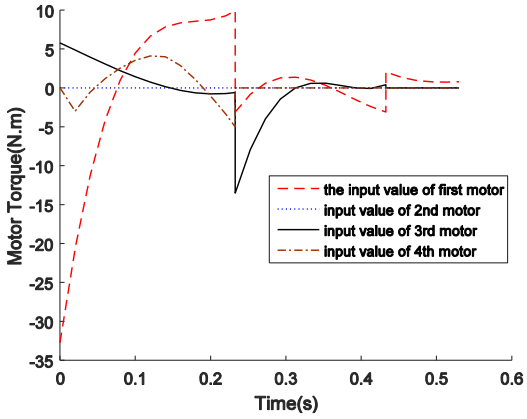

Fig. 13. Motors torque profiles for the springy semi-telescopic leg robot.

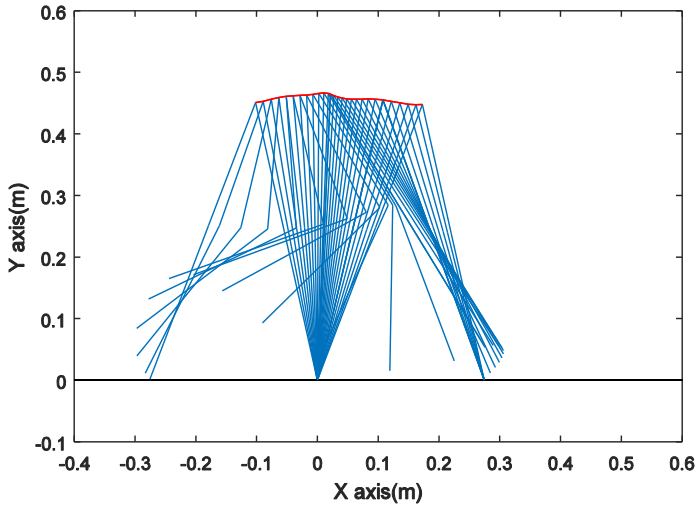

Fig. 14. Walking gait for the springy semi-telescopic biped.

3.4 The semi-compass gait robot with kneed swing leg

Again, successive optimizations are used to find an energy efficient periodic gait for the semi-compass gait robot model with kneed swing leg. The resulted torque profiles of the motors for this model are shown in Fig. 15. There is only one discontinuity in this graph related to the switching between the single support sub-phases. There is no continued double support phase for this model. This figure shows that the motors of the thigh and shin of the swing leg during the single support phase do not need noticeable torque values, but motor 1 for the stance leg thigh needs bigger torques to accelerate the robot mass for a periodic motion.

Fig. 16 illustrates the stick diagram for a full cycle of this model for periodic walking gait; the COT is 0.91.

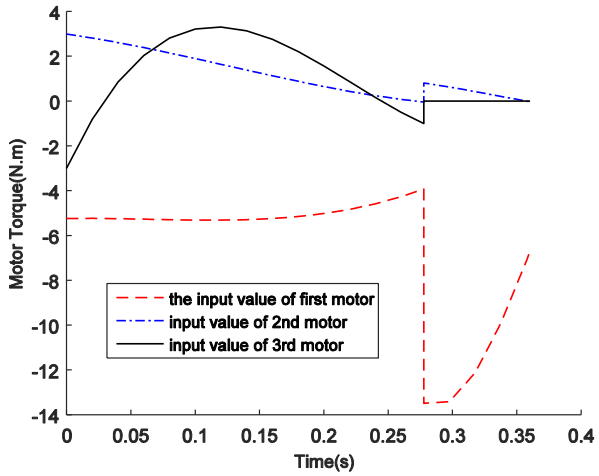

Fig. 15. Torque profiles for motors of semi-compass biped.

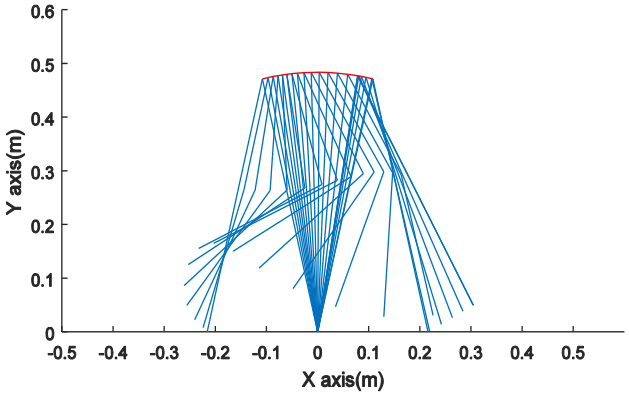

Fig. 16. Motion graph for semi-compass robot

4. Comparison of the Robot Models

The cost of transport gives a useful understanding of the robot's energy expenditure, therefore many researchers use this criteria to compare robots (Sellers et al., 2005). Our robot's total mass is 4.076 kg and a velocity of 0.6 *m/s* is considered for all models. Table 1. Summarizes the COT, Error, and velocity comparison for the different models. The reason that error of the semi-compass robot is small is because of its lower degrees of freedom and not using a passive and non-controllable spring element in its configuration. It is important to note that the robot's configuration is underactuated in springy versions. While the ideal compass gait model has passive walking gaits with COT of zero, and for its active gaits with different step length and forward velocity optimized gaits have been generated with COT less than 0.02 (An et al 2015), our model has much higher COT at the order of real robots. This is because our model possesses real-world condition such as a kneed swing leg to clear the ground.

Table 1. Comparing different models of robots

Robot Model	Velocity (*m/s*)	Error	COT ($J.N^{-1}m^{-1}$)
Kneed without spring	0.6	0.19000	0.6658
Kneed with springy shin	0.6	1.3129	4.267
Springy semi-telescopic robot	0.6	0.00320	1.0945
Semi-compass gait robot	0.6	0.00006	0.9146
Human (Soo & Donelan, 2010)	-	-	0.3
ASIMO Robot (Collins et al., 2005; Y. Sakagami et al., 2002)	-	-	3.2
MIT Robot (Tucker, 1975)	-	-	10.5
Delft Robot (Collins et al., 2005; Y. Sakagami et al., 2002)	-	-	5.3

From the COT point of view, the robots are ranked from the best to the worst as the kneed robot without spring, semi-compass gait robot with kneed swing leg, semi-telescopic leg robot with kneed swing leg, and kneed robot with springy shins. There is no motor to control telescopic joints in springy versions of the robot models. Motors act indirectly to control springs' deformation and their speed, which makes optimization inefficient. During the running gait of the springy semi-telescopic biped, when the front leg of the robot hits the ground, impact and inertia forces resulted from the impact are stored in the spring. This stored energy is used to pass the robot from the support point and saves some energy, but during walking motion, the spring force is not used efficiently for the next phase and results in a waste of energy.

The error for the kneed models with a higher degree of freedom is higher since the dynamic of the system is more complicated and the optimization parameters are more. The kneed robot also has the lowest COT which shows the advantages of the kneed leg in humans and animals. This is mainly because in the semi-telescopic and semi-compass biped robot, the stance leg motor should apply a larger toque to move the body around the whole leg, compared to the kneed robot that the stance leg is divided by the knee and the torques are distributed more efficiently. Table 1. compares the models in this project with the works of others. Our models have reasonable and less cost of transports relative to the other real multibody biped robots.

Conclusion

This research focuses on generating realistic gaits for the theoretic biped models extended to practical ones while optimizing the performance of the robot. To reach this goal, different architectures of a real biped robot were studied. These models are kneed biped robot without spring, kneed biped with springy shins, springy semi-telescopic robot, and semi-compass robot with kneed swing leg. All walking phases of these robots were modeled. Initial conditions and torque of the motors were calculated by solving optimization problems to find periodic gaits with a minimum cost of transport.

Based on the results of the simulation, the most efficient robot structure considering the cost of transport for planar walking with a constrained angle of the torso is the kneed biped robot without spring. Surprisingly, this standard kneed biped model has better performance in walking of a multibody robot than semi-compass gait and semi-telescopic springy leg robot. Although the theoretic compass gait model and SLIP model have high efficiencies, they neglect how the swing leg clears the ground. The main contribution of this work is to extend these theoretic models to real-world conditions and comparing their efficiencies with the standard kneed mechanism. The semi-compass and springy semi-telescopic robot models stand on a straight leg and push the body forward and at the same time, the other leg bends the knee and clears the ground. The walking gait of the semi-compass robot had the second rank regarding the COT. This was mainly because moving and straightening the kneed swing leg in a real way increased the COT. The springy semi-telescopic robot although has a good performance from the energy point of view in running mode, by storing and releasing the energy of the motors in the stance leg spring, it is not efficient in walking mode. The presence of the springs caused uncontrollable motions and wasted the energy of the motors; consequently increasing the COT. For the kneed robot with spring, because of the nonlinearity and presence of two springs in the shins of the robot, motors could not control the robot properly. Spring's deflection wasted a portion of the energy from the motors and made the robot not energy efficient. Due to all these issues, optimized gait had the worst efficiency.

Optimizing spring stiffnesses of the different models investigated in this work can be done in future works to explore more optimal models and gaits.

References

Adolfsson, J., Dankowicz, H., & Nordmark, A. (2001). 3D Passive Walkers: Finding Periodic Gaits in the Presence of Discontinuities. *Nonlinear Dynamics*, *24*(2), 205–229. https://doi.org/10.1023/A:1008300821973

Bauer, F., Römer, U., Fidlin, A., & Seemann, W. (2016). Optimization of energy efficiency of walking bipedal robots by use of elastic couplings in the form of mechanical springs. *Nonlinear Dynamics*, *83*(3), 1275–1301. https://doi.org/10.1007/s11071-015-2402-9

Collins, S., Ruina, A., Tedrake, R., & Wisse, M. (2005). Efficient Bipedal Robots Based on Passive-Dynamic Walkers. *Science*, *307*(5712), 1082. https://doi.org/10.1126/science.1107799

Dadashzadeh, B., Mahjoob, M. J., Nikkhah Bahrami, M., & Macnab, C. (2014). Stable active running of a planar biped robot using Poincare map control. *Advanced Robotics*, *28*(4), 231–244. https://doi.org/10.1080/01691864.2013.865299

Dadashzadeh, B., Mostafavi, S. A., & Allahverdizadeh, A. (2019). Dynamic Modeling and Optimal Walking Gait Planning of a Real Biped Robot Based on SLIP and Compass gait Models. *Journal of Applied and Computational Sciences in Mechanics*, *30*(1).

Gamus, B., & Or, Y. (2015). Dynamic Bipedal Walking under Stick-Slip Transitions. *SIAM Journal on Applied Dynamical Systems*, *14*, 609–642. https://doi.org/10.1137/140956816

Geyer, H., Seyfarth, A., & Blickhan, R. (2006). Compliant leg behaviour explains basic dynamics of walking and running. *Proceedings. Biological Sciences*, *273*(1603), 2861–2867. PubMed. https://doi.org/10.1098/rspb.2006.3637

Hao, Z., Fujimoto, K., & Zhang, Q. (2020). Approximate Solutions to the Hamilton-Jacobi Equations for Generating Functions. *Journal of Systems Science and Complexity*, *33*(2), 261–288. https://doi.org/10.1007/s11424-019-8334-6

Hu, Y., Yan, G., & Lin, Z. (2011). Stable running of a planar underactuated biped robot. *Robotica*, *29*(5), 657–665. Cambridge Core. https://doi.org/10.1017/S0263574710000512

Kai, T., & Shibata, T. (2015). Gait Generation for the Compass-Type Biped Robot on General Irregular Grounds Via a New Blending Method of Discrete Mechanics and Nonlinear optimization. *Journal of Control, Automation and Electrical Systems*, *26*. https://doi.org/10.1007/s40313-015-0192-4

L. C. Visser, S. Stramigioli, & R. Carloni. (2013). Control strategy for energy-efficient bipedal walking with variable leg stiffness. *2013 IEEE International Conference on Robotics and Automation*, 5644–5649. https://doi.org/10.1109/ICRA.2013.6631388

Martin, A. E., & Schmiedeler, J. P. (2014). Predicting human walking gaits with a simple planar model. *Journal of Biomechanics*, *47*(6), 1416–1421. https://doi.org/10.1016/j.jbiomech.2014.01.035

McGeer, T., & Alexander, R. M. (1990). Passive bipedal running. *Proceedings of the Royal Society of London. B. Biological Sciences*, *240*(1297), 107–134. https://doi.org/10.1098/rspb.1990.0030

Millard, M., Kubica, E., & McPhee, J. (2011). Forward dynamic human gait simulation using a SLIP target model. *IUTAM Symposium on Human Body Dynamics*, *2*, 142–157. https://doi.org/10.1016/j.piutam.2011.04.015

Rokbani, N., & Alimi, A. (2012). *IK-PSO, PSO Inverse Kinematics Solver with Application to Biped Gait Generation*. https://doi.org/10.5120/9432-3844

Rostami, M., & Bessonnet, G. (2001). Sagittal gait of a biped robot during the single support phase. Part 2: Optimal motion. *Robotica*, *19*(3), 241–253. Cambridge Core. https://doi.org/10.1017/S0263574700003039

Rummel, J., Blum, Y., & Seyfarth, A. (2010). Robust and efficient walking with spring-like legs. *Bioinspiration & Biomimetics*, *5*(4), 046004. https://doi.org/10.1088/1748-3182/5/4/046004

S. Shimmyo, T. Sato, & K. Ohnishi. (2010). Biped walking pattern generation by using preview control with virtual plane method. *2010 11th IEEE International Workshop on Advanced Motion Control (AMC)*, 414–419. https://doi.org/10.1109/AMC.2010.5464096

Saidouni, T., & Bessonnet, G. (2003). Generating globally optimised sagittal gait cycles of a biped robot. *Robotica*, *21*(2), 199–210. Cambridge Core. https://doi.org/10.1017/S0263574702004691

Sellers, W. I., Cain, G. M., Wang, W., & Crompton, R. H. (2005). Stride lengths, speed and energy costs in walking of Australopithecus afarensis: Using evolutionary robotics to predict locomotion of early human ancestors. *Journal of the Royal Society, Interface*, *2*(5), 431–441. PubMed. https://doi.org/10.1098/rsif.2005.0060

Soo, C. H., & Donelan, J. M. (2010). Mechanics and energetics of step-to-step transitions isolated from human walking. *The Journal of Experimental Biology*, *213*(24), 4265. https://doi.org/10.1242/jeb.044214

Srinivasan, M., & Ruina, A. (2006). Computer optimization of a minimal biped model discovers walking and running. *Nature*, *439*(7072), 72–75. https://doi.org/10.1038/nature04113

Tucker, V. A. (1975). The Energetic Cost of Moving About: Walking and running are extremely inefficient forms of locomotion. Much greater efficiency is achieved by birds, fish—And bicyclists. *American Scientist*, *63*(4), 413–419. JSTOR.

Sakagami Y., Watanabe R., Aoyama C., Matsunaga S., Higaki N., & Fujimura K.. (2002). The intelligent ASIMO: system overview and integration. *IEEE/RSJ International Conference on Intelligent Robots and Systems*, *3*, 2478–2483 vol.3. https://doi.org/10.1109/IRDS.2002.1041641

An, K., and Chen, Q. (2015). Dynamic optimization of a biped model: Energetic walking gaits with different mechanical and gait parameters. Advances in Mechanical Engineering, Vol. 7(5) 1–13, DOI: 10.1177/1687814015583041

(Liu et al., 2019)

(Mandava et al., 2019)